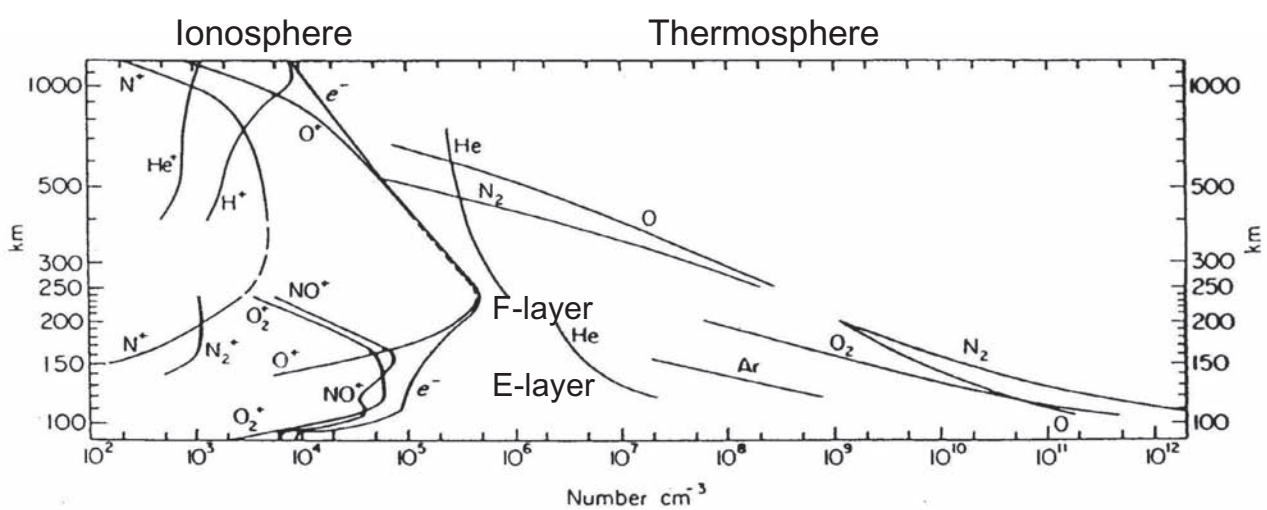


# 熱圏大気における酸素原子分布と運動

渡部重十, 栗原純一(北海道大学)  
 和田智之(理化学研究所)  
 山本真行(高知工科大学)  
 岩上直幹(東京大学)



**Fig. 1.2.** International Quiet Solar Year (IQS) daytime atmospheric composition, based on mass spectrometer measurements above White Sands, New Mexico ( $32^{\circ}\text{N}$ ,  $106^{\circ}\text{W}$ ). The helium distribution is from a nighttime measurement. Distributions above 250 km are from the Elektron II satellite results of Istomin (1966) and Explorer XVII results of Reber and Nicolet (1965). [C. Y. Johnson, U.S. Naval Research Laboratory, Washington, D.C. Reprinted from Johnson (1969) by permission of the MIT Press, Cambridge, Massachusetts. Copyright 1969 by MIT.]

Although the ionization rate is  $<10^{-4}$  in the low latitude thermosphere, the dynamics of the neutral atmosphere is strongly controlled by the plasma.

# Global Change of Ionosphere

## Global Worming / Global Cooling

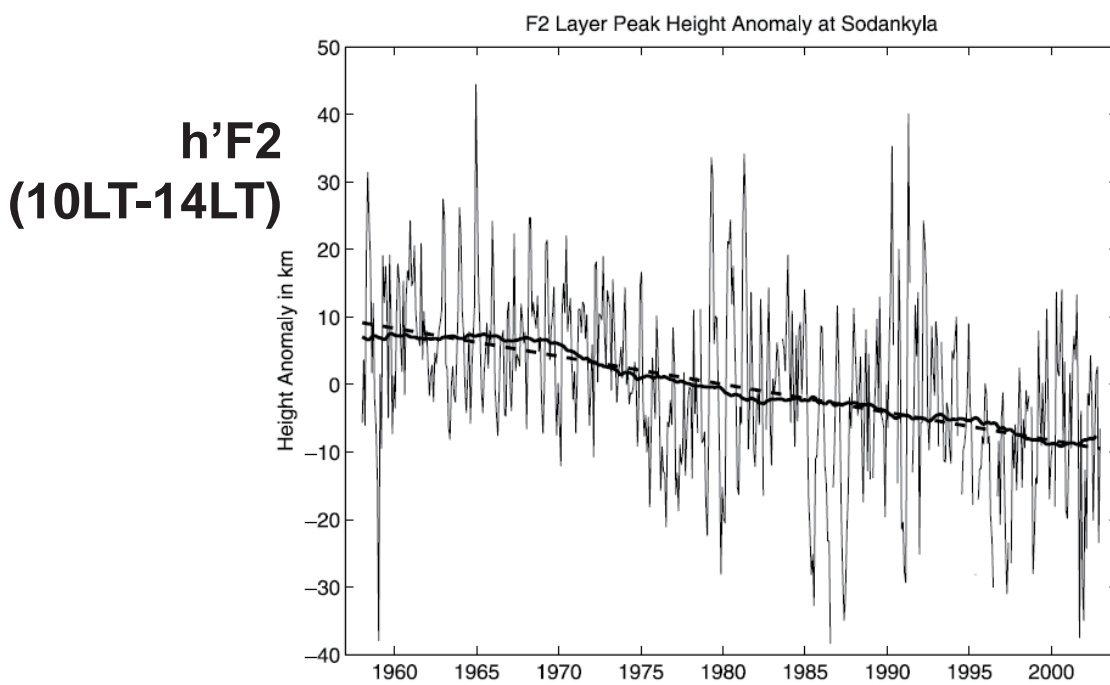
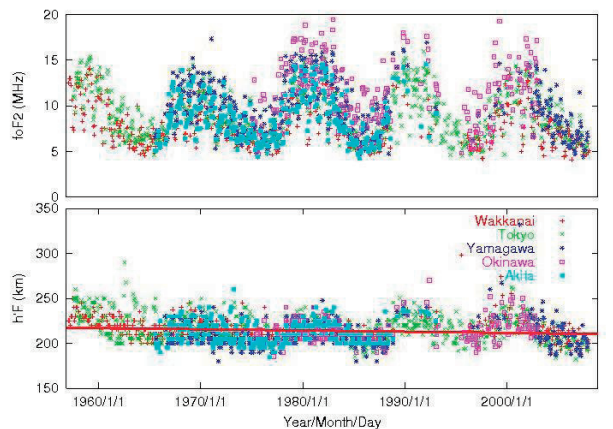


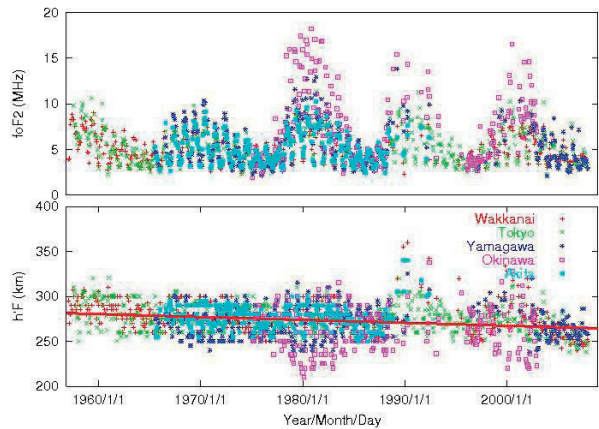
Fig. 1. The plot shows the monthly median  $h'mF2$  anomaly (10LT-14LT) at Sodankylä ( $68^{\circ}N$ ,  $27^{\circ}E$ ), 1958–2003 (thin line), with the 11-year running mean (thick line) and the linear least-square fit (dashed line). The trend is  $-0.41 \pm 0.04$  km/yr.

Ulich and Turunen, 1997

## Ionosphere over Japan for 60 years



Day (10LT-15LT)



Night (22LT-3LT)

10~20kmの電離層高度減少  $\Rightarrow$   $\sim 100k$ の熱圏大気温度減少

## Longitudinal Structure of Ionosphere

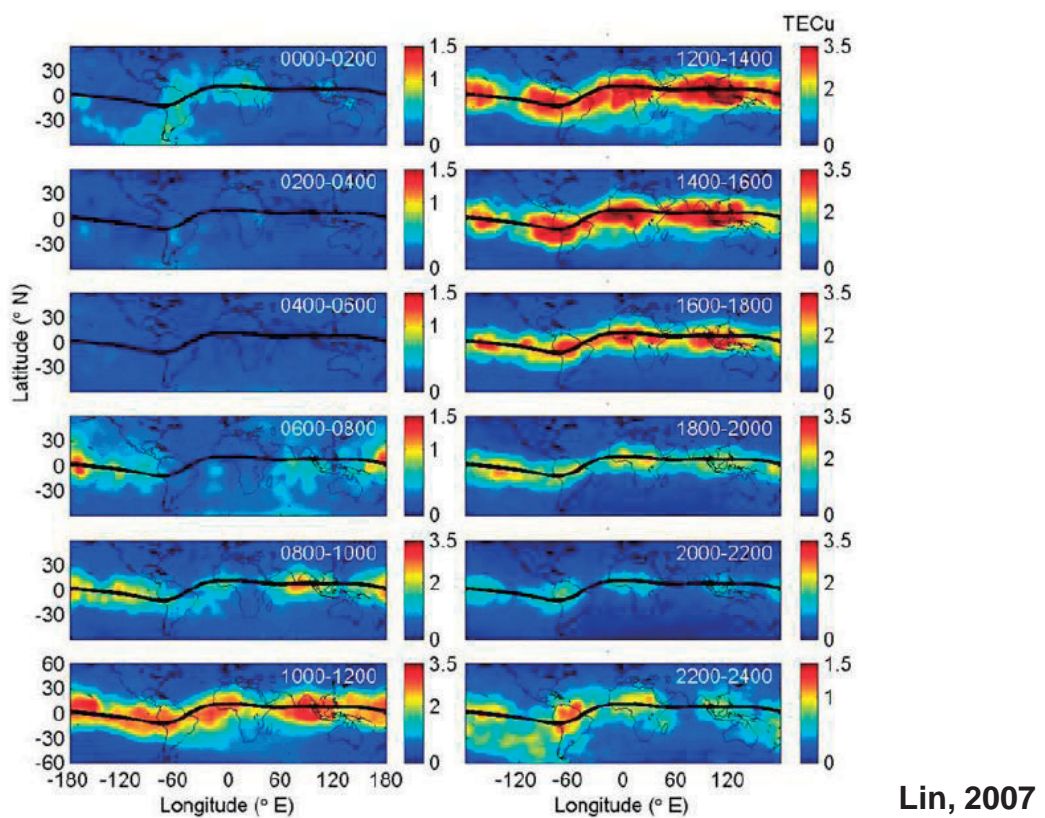


**Figure 1.** Temporal variations of the four-peaked longitudinal structure of integrated total electron content between 400 and 450 km in 2-h segments. It is noted that the color contour levels are varying in different subplots in order to clearly show the four-peaked structure.  $1\text{TECu} = 10^{12}\text{ electrons/cm}^2$ .

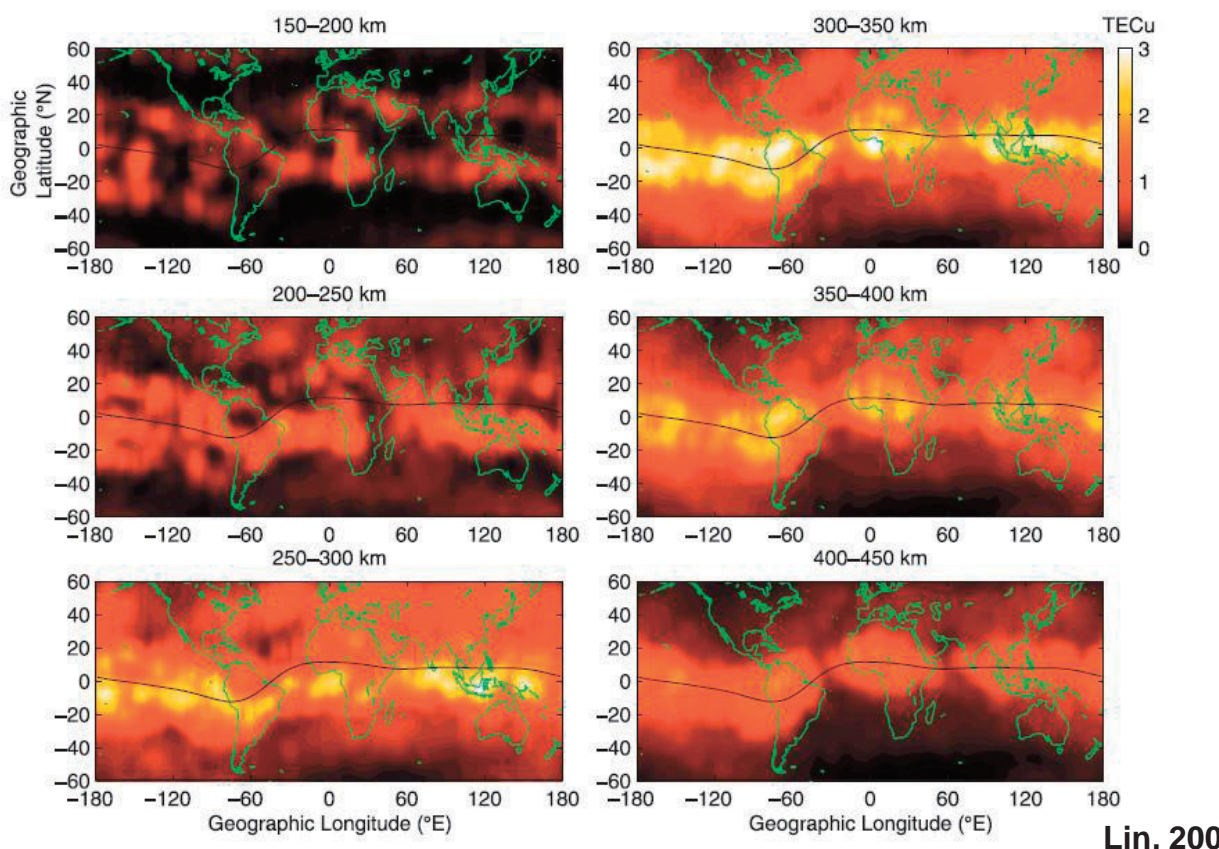


**Figure 3.** Integrated electron content at every 50 km altitude interval from 150 km to 450 km altitude observed by the FORMOSAT-3/COSMIC during 2000–2200 local time period during around September Equinox, 2006.

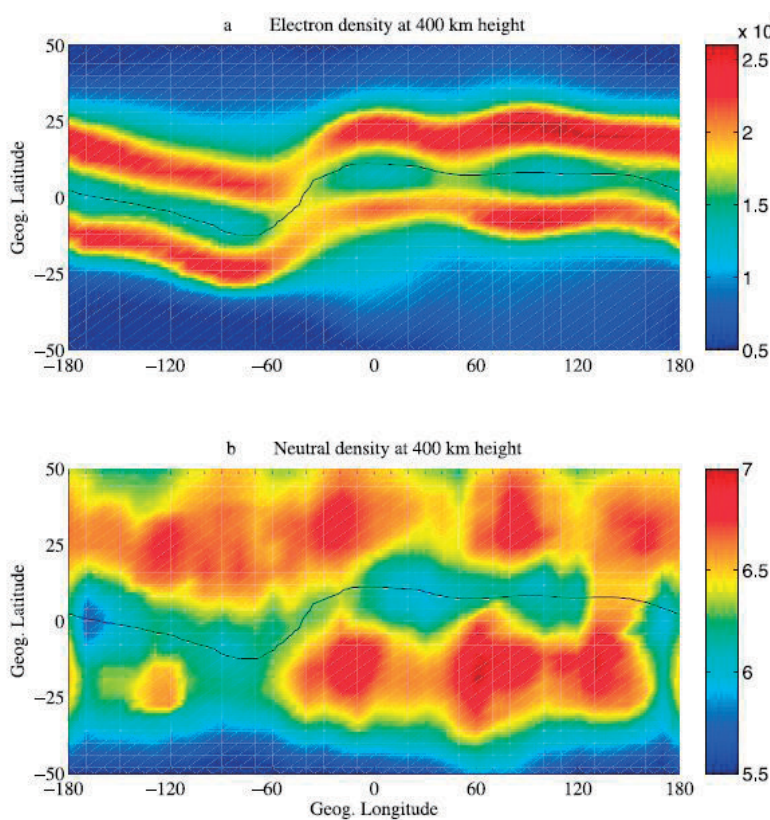
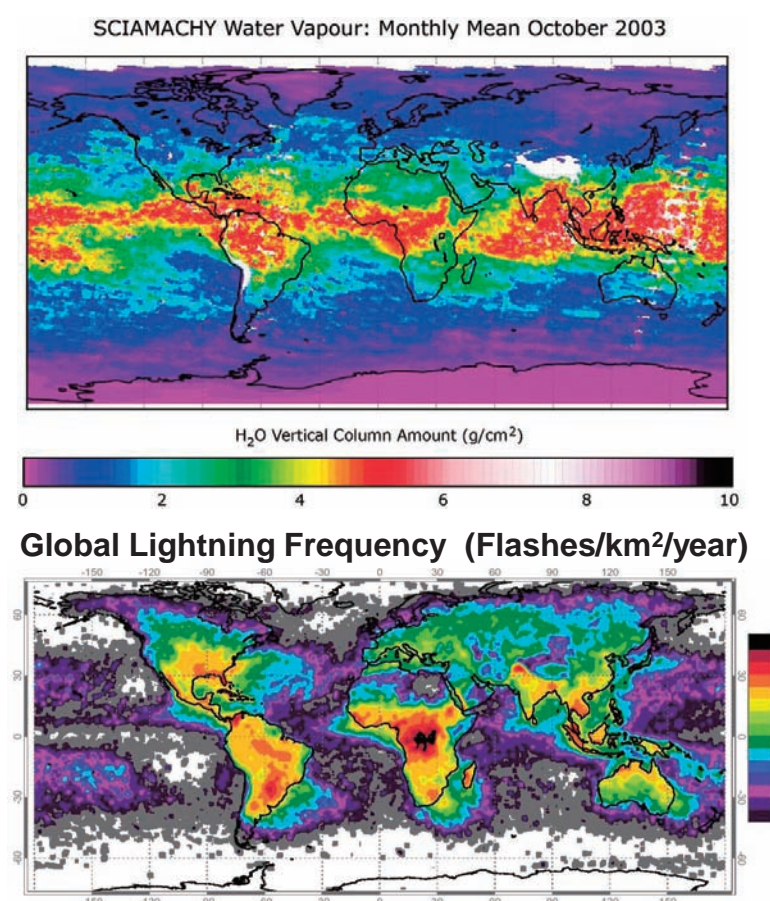
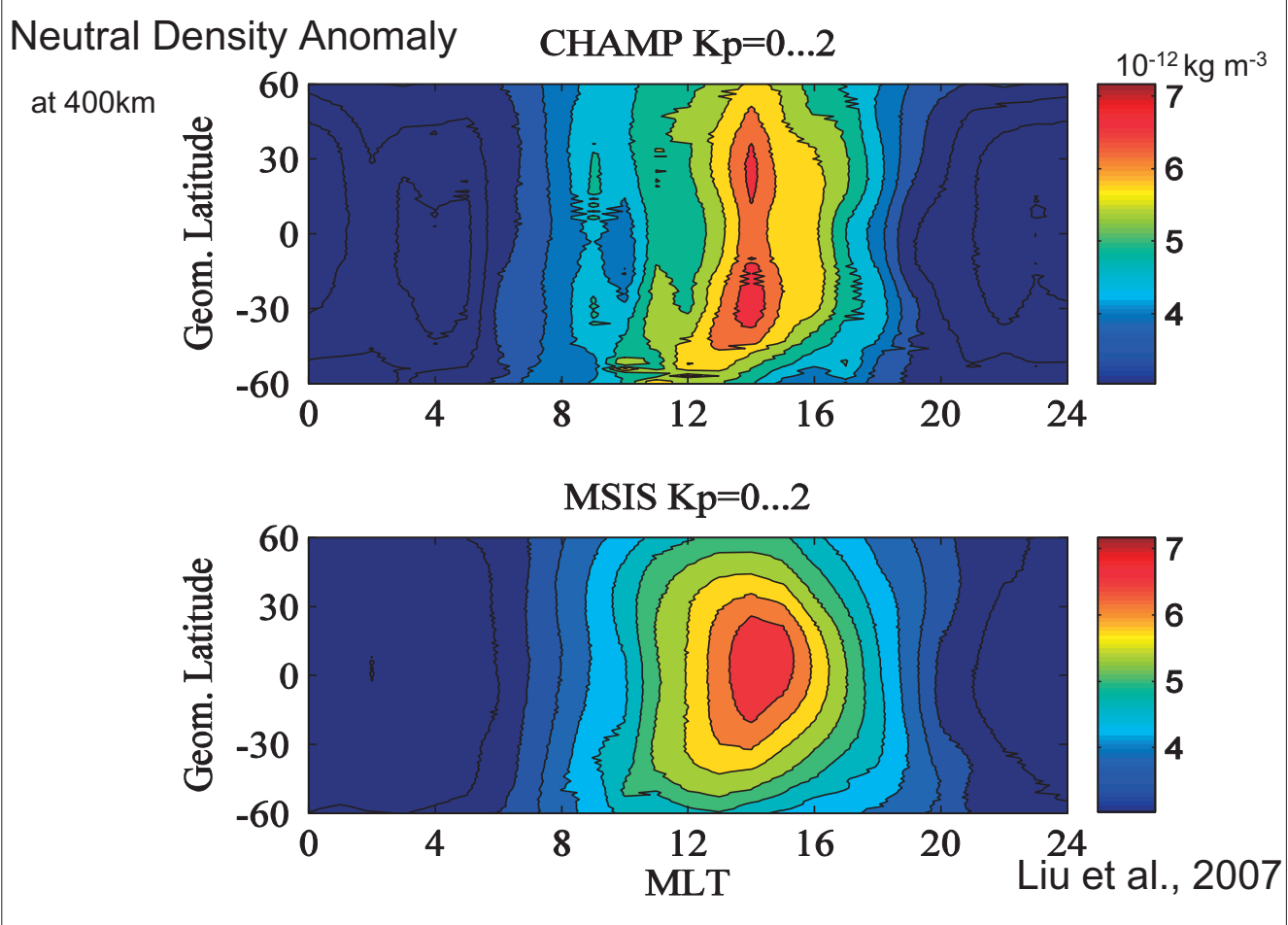


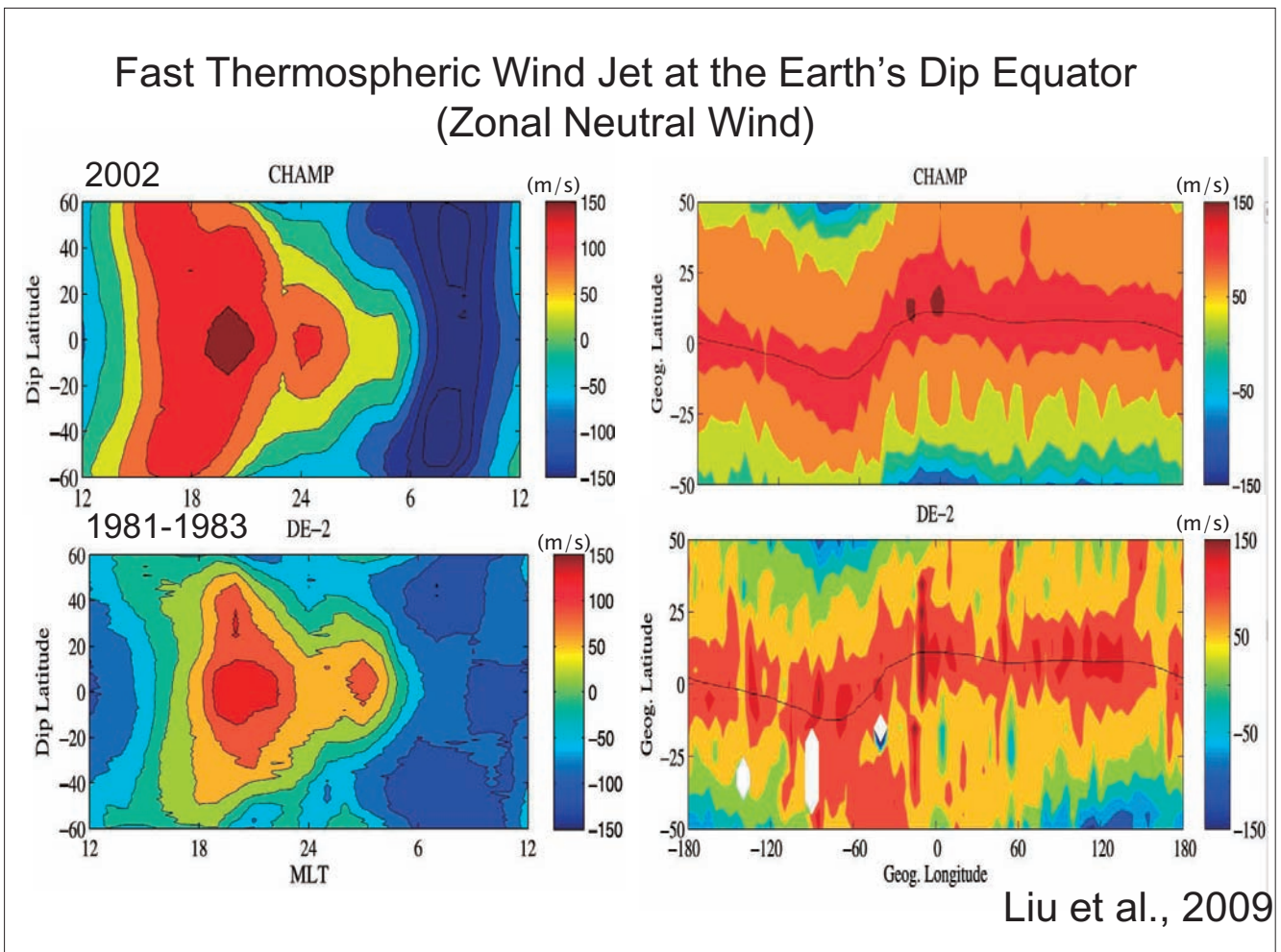
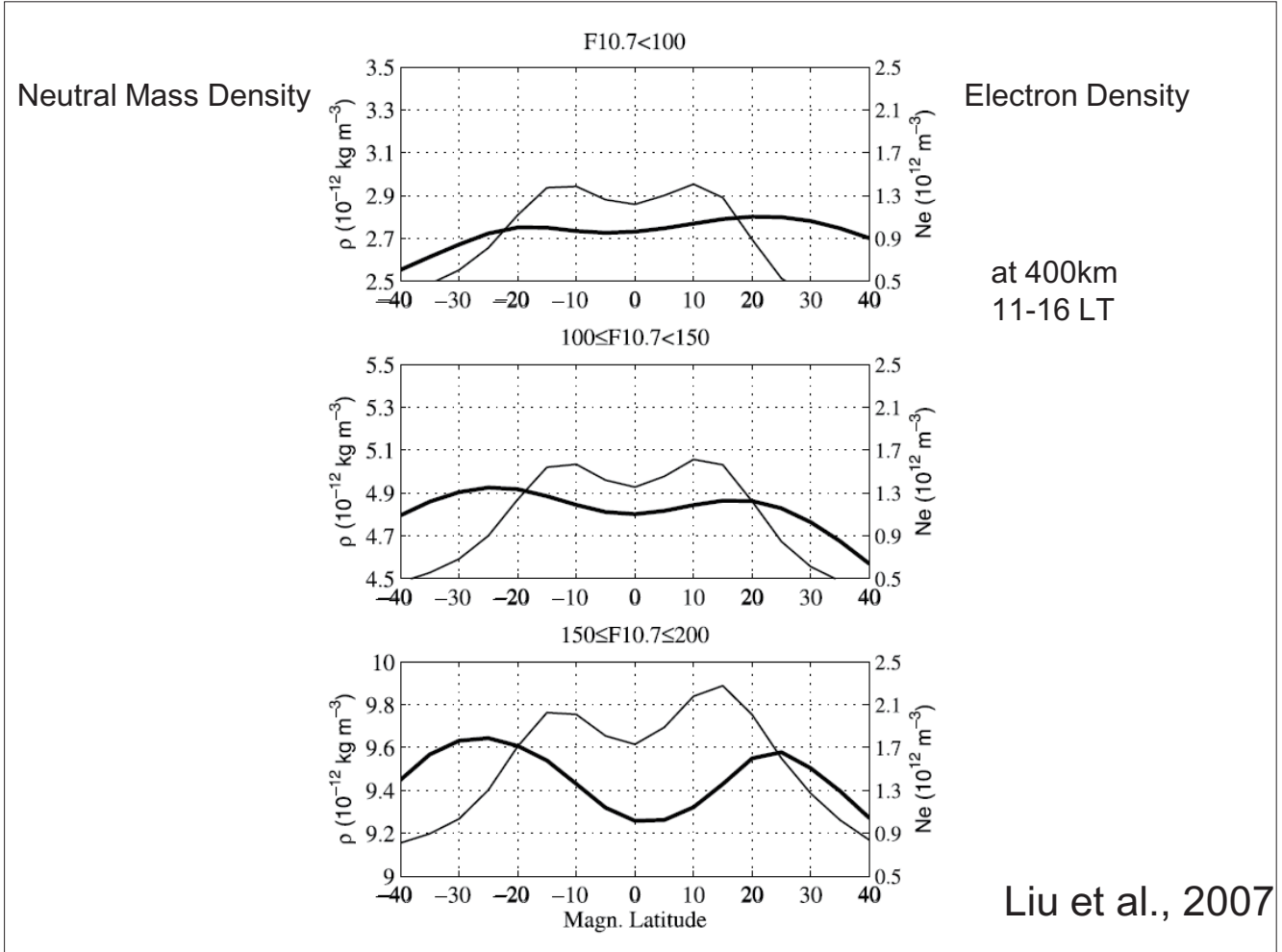
Figure 1. Distribution of the (a) electron density in unit of  $\text{cm}^{-3}$  and (b) neutral density in unit of  $10^{-12} \text{ kg}$  during 14–18 LT in the geographic coordinates near equinoxes in 2002.

Liu et al., 2009



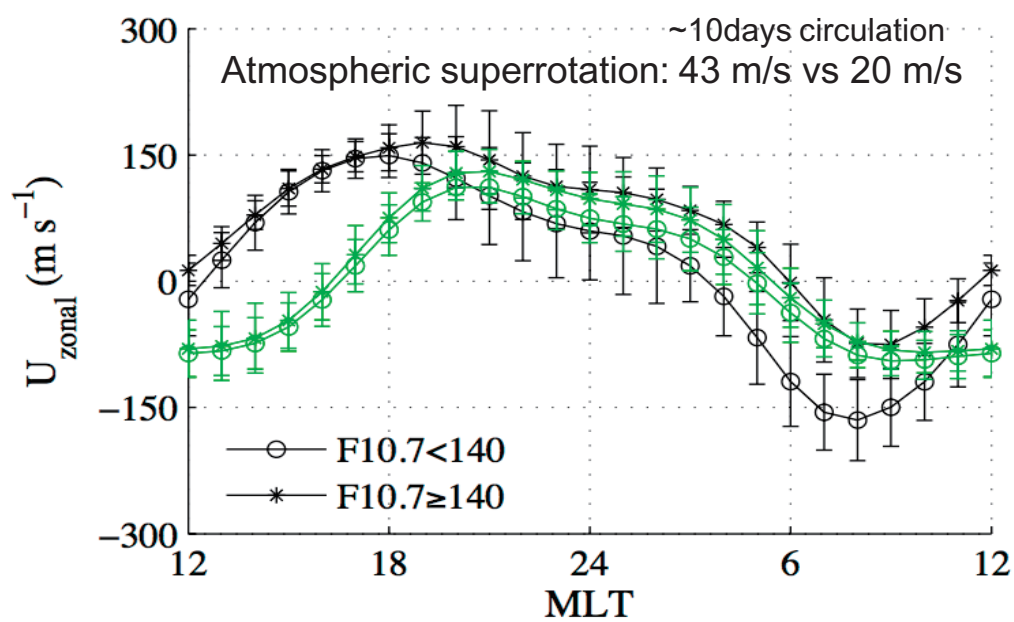
# Ionosphere-Thermosphere Coupling





# Super-rotation of Atmosphere and Plasma

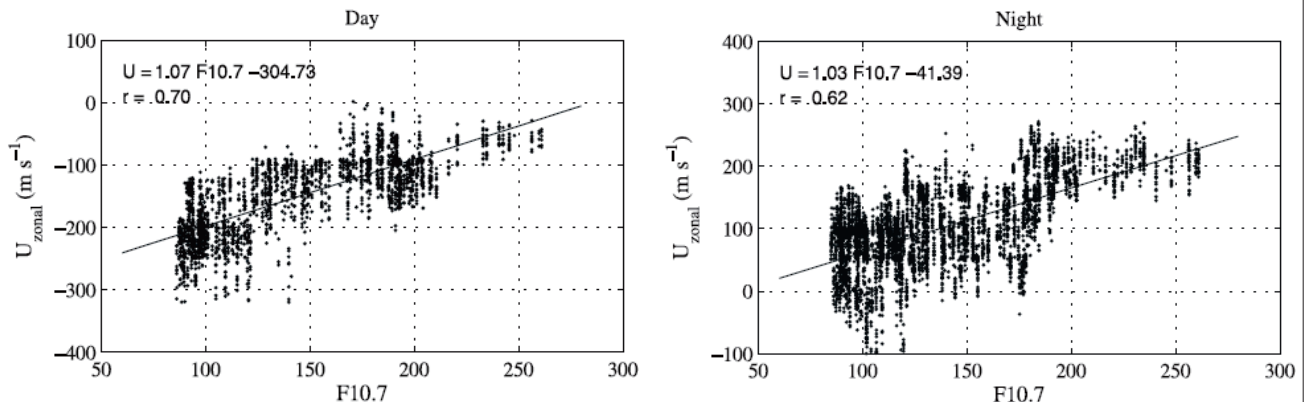
## Wind Diurnal Variation: CHAMP vs HWM



Average zonal wind between 10 S ~ 10 N. Green line: HWM; Black lines: CHAMP. Good agreement at high solar flux levels on the night side, but a 3-4 hours phase shift between two sets.

Liu et al., 2006

## Atmospheric Super-rotation at 400 km altitude



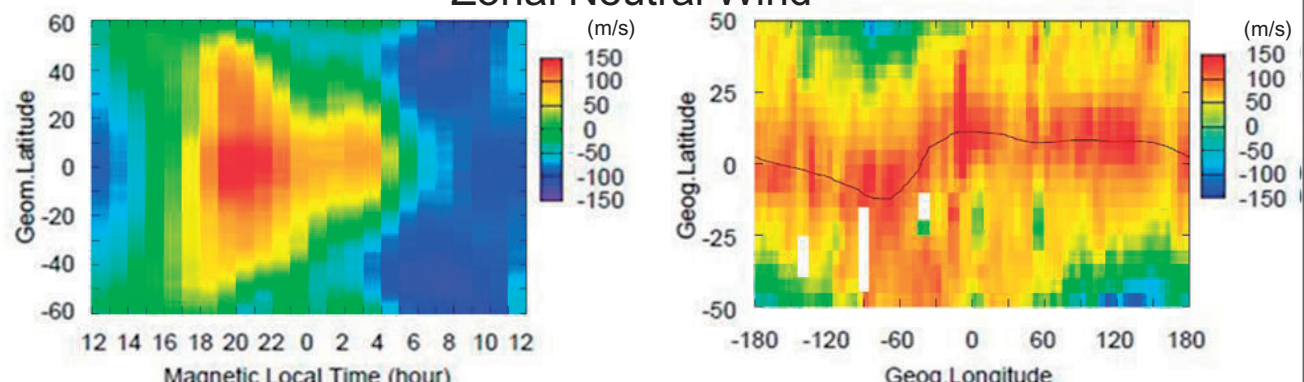
	Summer	Equinox	Winter	Average
<b>F10.7&lt;140</b>	11	22	34	22
<b>F10.7&gt;140</b>	40	72	76	63

fastest in winter at high solar flux level

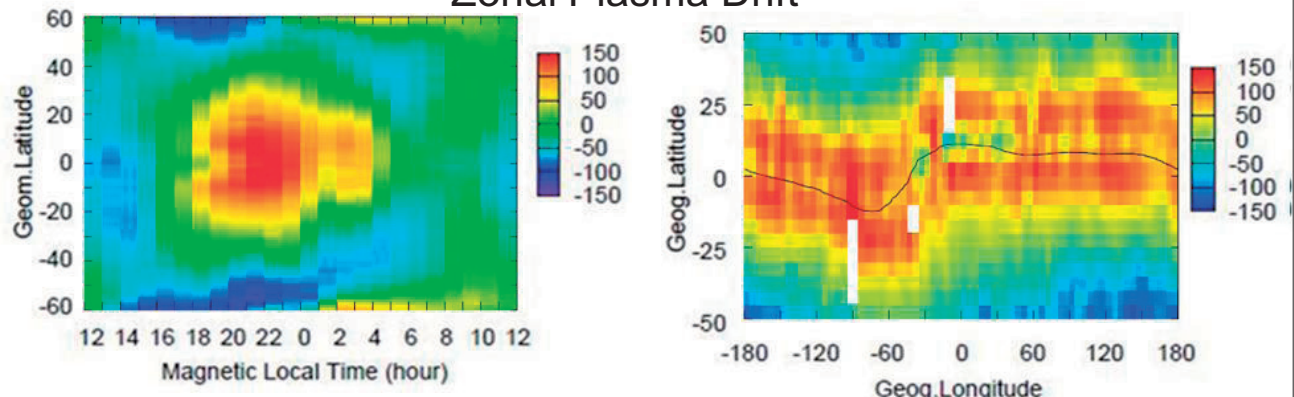
Liu et al., 2006

DE2

### Zonal Neutral Wind



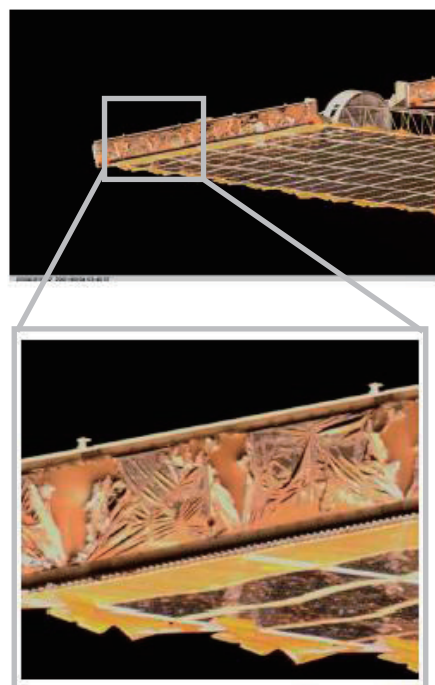
### Zonal Plasma Drift



# Measurement of Atomic Oxygen

## 酸素原子観測の重要性

- ・ 高度200～400km:  
宇宙ステーションや  
低軌道衛星(LEO)の  
深刻な表面劣化
- ・ 高度100～200km:  
酸素原子の生成・消滅が  
あらゆる大気化学反応に影響



(Banks et al., 2002)

# 酸素原子の主な観測法

- ・質量分析計: 高速だが大型
- ・水晶質量センサ(QCM): 小型だが低寿命
- ・共鳴散乱法: 高速だが不正確



e-POP/NMS

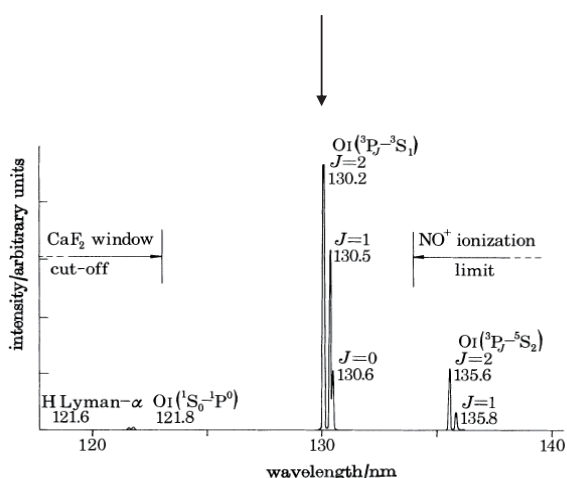


QCM

→ 高速で正確な観測手法と小型な観測装置が求められている

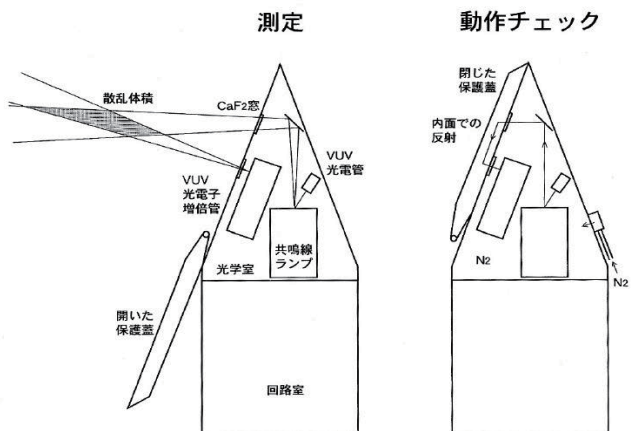
## 観測ロケット用 酸素原子共鳴散乱法

### 酸素原子共鳴(三重)線



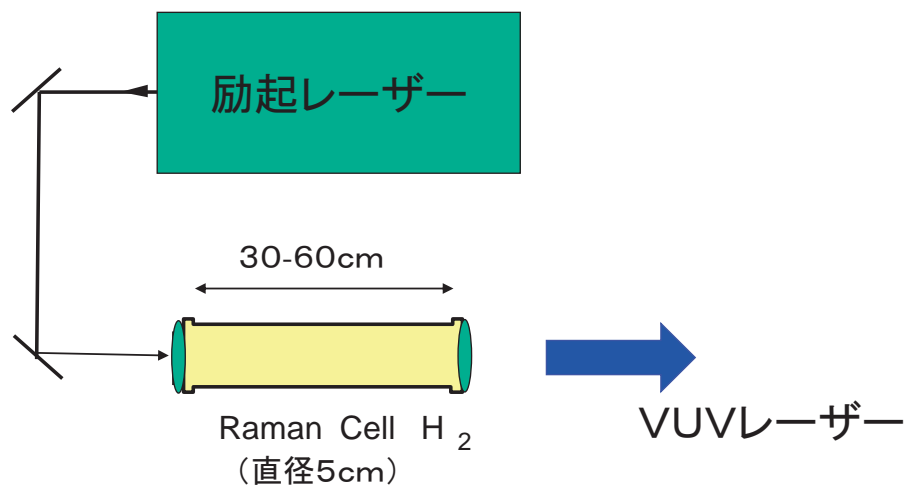
(Dickinson et al., 1980)

### 観測ロケットS-310-29号機 搭載測定器



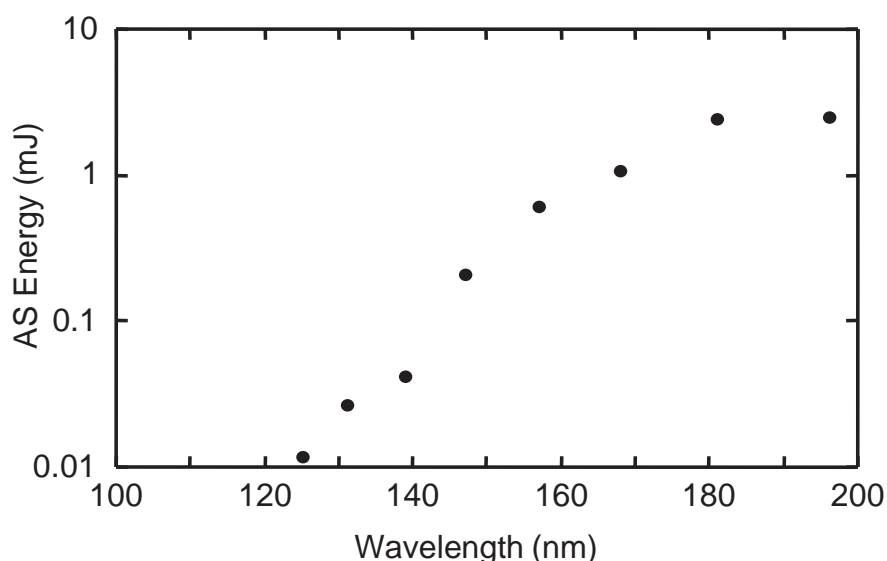
(岩上他, 2001)

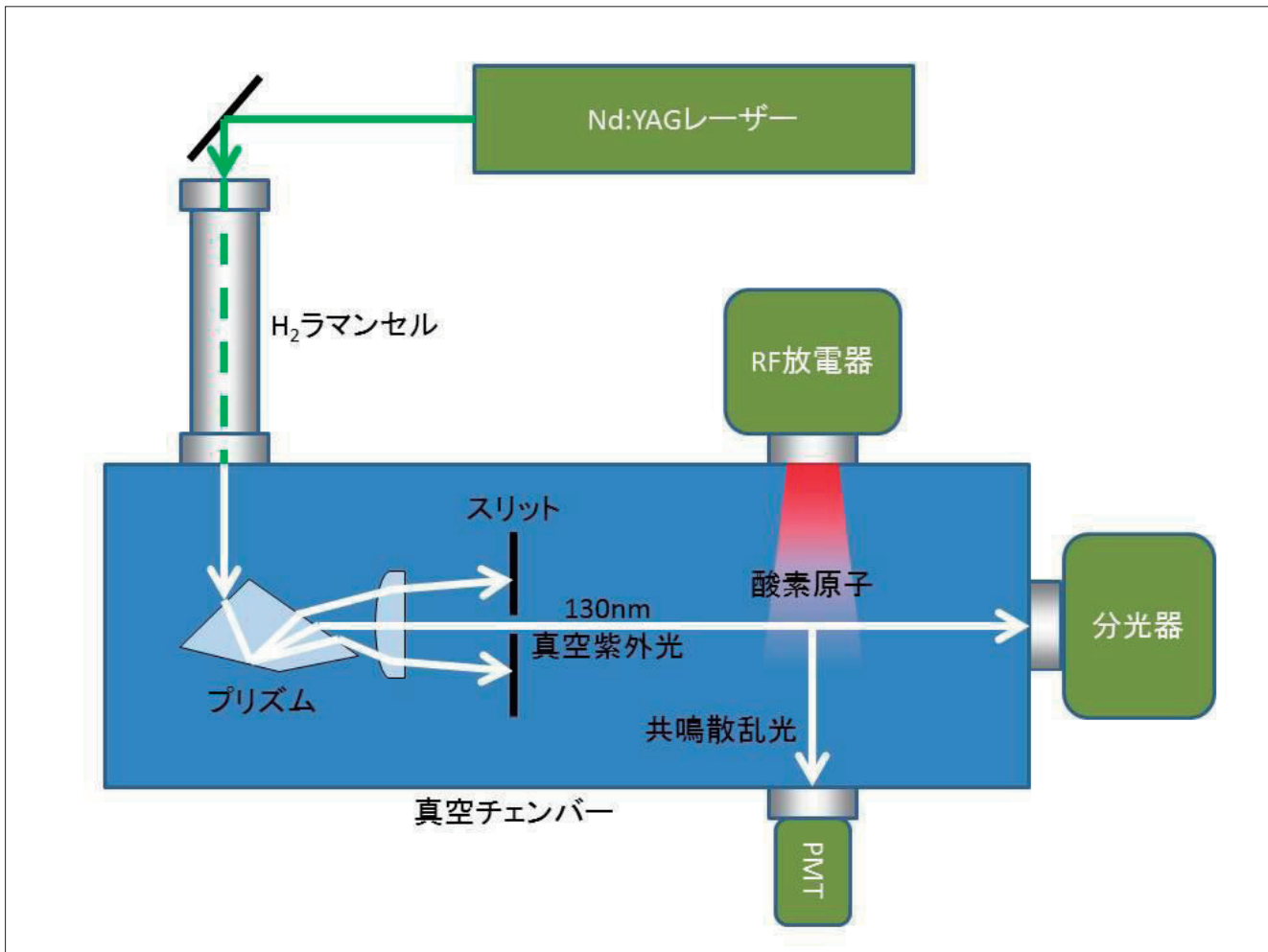
## 宇宙実験でのレーザーシステム



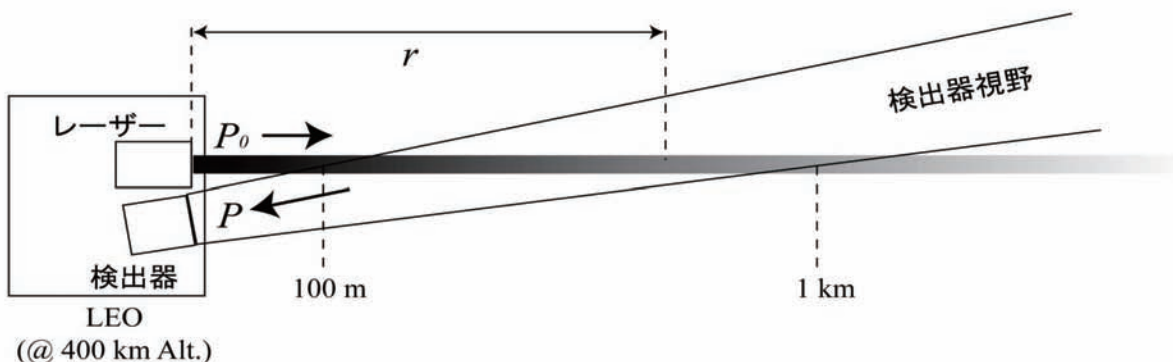
小型のセルを挿入するだけで、真空紫外線が発生する。  
励起レーザーが重要

### 真空紫外反ストークス光出力例





## 衛星搭載用 酸素原子密度測定器



後方散乱強度Pについてのライダー方程式

$$P = P_0 n A \eta \sigma \int \frac{T^2}{r^2} dr$$

n:酸素原子密度    A:受光面積    η:検出器効率    σ:散乱断面積  
T:透過率

# 真空紫外レーザーの応用の利点

- 強い光強度によるS/N比の向上
- 高い指向性による観測領域の延伸
- 波長幅・波長可変によるドップラーシフトの低減
- パルス・レーザーによる昼夜観測